Research & Reviews: Journal of Engineering and Technology

e-ISSN: 2319-9873
p-ISSN: 2347-2324

Low-Profile Wideband Linear Polarized Patch Antenna Using Metasurface: Design and Characterization

Ashraf Sayed Abdel Halim

Department of Communication, Canadian International College (CIC) Cairo, Egypt

Research Article

Received date: 06/08/2019

Accepted date: 20/08/2019

Published date: 27/08/2019

*For Correspondence:

Department of Communication, Faculty of Engineering, Canadian International College (CIC) Cairo, Egypt.

E-mail: Ashraf_sayed@cic-cairo.com

Keywords: Low-profile antenna, Wideband patch antenna, Linearly polarized patch antenna

ABSTRACT

A low-profile wideband linear polarized patch antenna using meta-surface is suggested for the wideband procedure at 5-GHz Wi-Fi bands. The antenna consisted of a rectangular patch interceded between a grid of 3×3 periodic meta-surface and the ground plane. The accepted coaxial probe feed is uncomplicated to manufacture and match. Characteristic Mode Analysis (CMA) is used to evaluate and study the mechanism of action of the suggested antenna. We found that 2 main distinctive modes are effectively excited causing the broadband procedure and linearly polarized radiation. The suggested dielectric-filled antenna with a low profile of 0.057 λ_0 (λ_0 is the working wavelength at 5.7 GHz in free space) gains about 30% calculated -10 dB impedance bandwidth (4.89-6.62 GHz) with 7.28 dBi median achievement. Over the bandwidth, the antenna performance is >90%, and cross-polarization levels are <18 dB.

INTRODUCTION

Micro-Strip Antennas (MSAs) are prevalent and favored in wireless communication systems, mobile, GPS, armed goals, satellite communication, for its attractive characteristics of low profile, less complicated, lightweight, simple manufacture, and definite assurance. But micro-strip antennas also have drawbacks like a small achievement, limited effectiveness, small bandwidth because of its innate feature. Many researches have been carried out on elevating the bandwidth of various microstrip antennas [1-4]. But, it is complex to attain wide bandwidth when sustaining low profile. Metasurface (MTS) as an encouraging resolve has been investigated to exaggerate the bandwidth and several patch antennas utilizing metasurface have been introduced for low profile and broadband procedure [5-8]. A lot of techniques involving equivalent circuits [9,10], effective medium theory [11], surface impedance extraction [12,13] and modal dispersion curve [14,15] are utilized to delineate the engineered metasurface. However these, techniques are inappropriate for investigating antennas utilizing metasurface composed of few unit cells. The Theory of Characteristic Modes (TCM) established at the Moment Of Method (MOM) is actually a favorable technique for antenna plan due to the physical judgment it delivers into the radiating phenomena occurred in the antenna. The theory of characteristic modes has been opportunely used to investigate and plan various antennas [16-21]. Lin et al. [22], used the theory of characteristic modes for the modeling, analysis, and judgment of a low-profile wideband metasurface antenna which is supplied by a microstrip line throughout aperture-coupling. In addition, Characteristic Mode Analysis (CMA) is utilized to inhibit the undesirable higher-order modes of the metasurface in multiport antenna systems for bettering the radiation act [23].

The aims of this study are planning a low-profile wideband microstrip antenna utilizing metasurface and use the CMA to examine and explain the mechanism of action of the suggested antenna. The antenna is composed of a rectangular patch in sandwiched the middle of the metasurface and the ground plane. The coaxial probe supplier is adopted, where the interior conductor of the coax is linked to the patch and the exterior conductor is linked to the ground plane. Comprehensive Modal Weighting Coefficients (MWC) with consideration of electric field coupling are measured to examine the broadband procedure and the radiation features.

e-ISSN: 2319-9873
p-ISSN: 2347-2324

MATERIAL AND METHODS

Characteristic Mode (CM) Theory For Antennas With Multi-Layered Medium

The conventional characteristic mode theory was first evolved for PEC objects in free space [24]. In contrast to the Electric Field Integral Equation (EFIE) for PEC objects in free space, the Mixed-Potential Integral Equation (MPIE) with spatial domain Green's Functions (GFs) of multi-layered medium are evolved for the established characteristic root equation [25]. The mixed-potential integral equation with spatial domain GFs of multi-layered medium gives the ability to precisely model the surface currents on metallic conductors entombed inside the multi-layered medium. The ground plane and dielectric substratum in the mixed potential integral equation is supposed to be perpetually in the transverse path. Keeping in mind the frame condition on the PEC, that is, the tangential ingredients of the electric field on the PEC surfaces are zero, the mixed-potential integral equation that assigns the unidentified current J and incident field Ei can be written as illustrated [26-29].

$$E^i_{tan} = [jw\mu_0(G_{a'}J) \quad -\frac{1}{j\omega\varepsilon_0}\nabla G_{q'}\nabla' . J_{tan} \qquad (1)$$

Where Ga and Gq are the spatial domain, GFs for the vector as well as scalar potentials, respectively. The closed-form term of the spatial domain GFs can be gained utilizing the discrete complex image method [26-31]. By employing the typical Galerkin's operation to the mixed-potential integral equation in (1), the matters of the sequel impedance matrix Z can be illustrated as follows:

$$Z_{mn} = jw\mu_0 \iint_{T_m} \iint_{T_n} f_m(r) . f_n(r') G_a(r, r') dr' d +$$

$$\frac{1}{jw\varepsilon_0} \iint_{T_m} \iint_{T_n} \nabla . f_m(r) \nabla' . f_n(r') G_q(r, r') dr' dr$$

Where fm (r) is the renowned RWG fundamental functions known over triangle pairs on the radiating patch. Following the operation of the conventional characteristic mode theory for PEC objects, a generalized eigenvalue equation for the mixed-potential integral equation can be written as follows: (2)

$$[X]J_n = \lambda_n[R]J_n$$

Where [R] and [X] are the actual and unreal components of the Moment Method impedance matrix Z, respectively. Eigenvector Jn and eigenvalue λ_n can be gained by solving (3). The modal significance (MS) is illustrated as follows:

$$MS = \frac{1}{1 + j\lambda_n} \qquad (3)$$

Peculiar modes form a full series of solutions, and thus the whole current can be shown as a linear superposed of these mode currents

$$J = \sum_n \alpha_n J_n \qquad (4)$$

Where α_n indicate the modal weighting coefficient (MWC) and can be calculated by (5)

$$\alpha_n = \frac{V'_n}{1 + j\lambda_n} = \frac{J_{n'}E^i}{1 + j\lambda_n}$$ The expression in (5) signifies the modal excitation coefficient, and Ei indicates the external excitation. Utilizing mutuality theorem,[32,33] the nominators in (6) can also be rewritten as follows: (6)

$$\left(J_{n'}E^i\right) = \left(E_{n'}J^i\right) = \int\int\int E_n . J^i dv$$

En indicates the electric field because of the modal current density Jn and Ji signifies an affected current density on a coupler. On the contrary, to a delta-gap voltage origin, if we utilize a probe as the coupler, the feed probe at the feed position can be modelled as a uniform current [33]. Employing this interpretation and replacement (7) into (6), the Modal Weighting Coefficient (MWC) with consideration to the probe feed coupling can be illustrated as follows: (7)

e-ISSN: 2319-9873
p-ISSN: 2347-2324

$\alpha_n = \frac{\left(J_n, E^i\right)}{1+j\lambda_n} = \frac{E_n(r_0)\cdot I}{1+j\lambda_n}$ Where r0 indicates the feed situation and I indicates the probe length. Thus we can utilize the (8) to calculate the modal weighting coefficient modal weighting coefficient of the suggested probe-feed metasurface antenna.

Antenna Design

The construction of the suggested antenna is illustrated in **Figure 1**. The antenna composed of 3 metal layers, the metasurface, the driven patch, and the ground from upper to lower. The thickness of the 2 F4BM350 substrates (r=3.5 and tan δ =0.001) is 1.5 mm. To obtain
a low profile and easy manufacture, 2 substrate layers stack with each other without air
gap. The internal part of the 50-SMA connector is connected to the patch and the external conductor is attached to the ground plane. The adopted metasurface is a periodic construction.

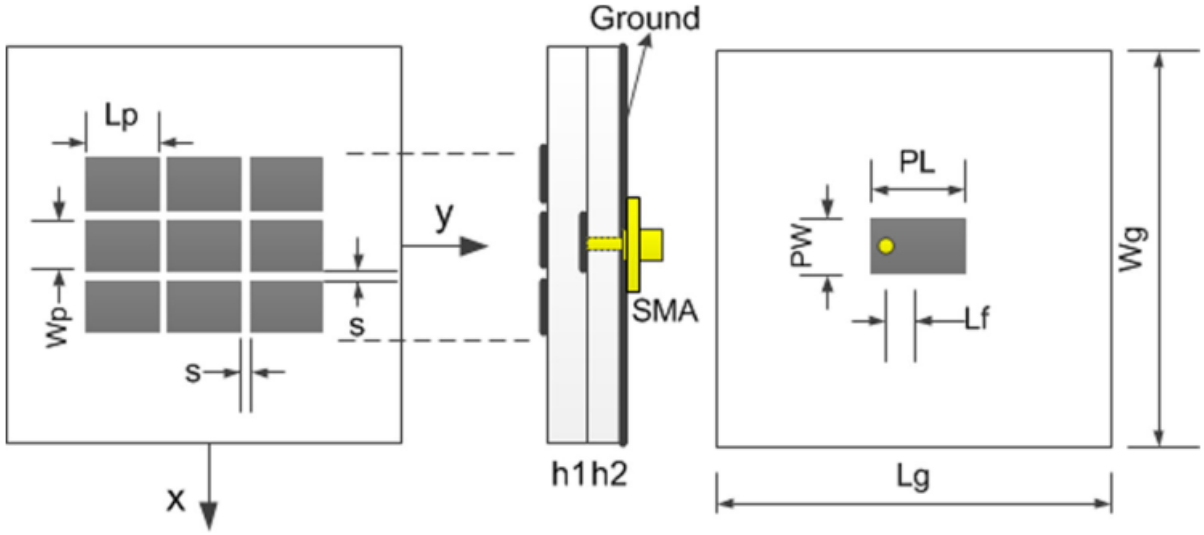

Figure 1. Construction of the suggested antenna.

Table 1. Measurements of the antenna (mm).

Lp	Wp	S	h1	h2	PL	PW	Lf	Lg	Wg
9.1	7	0.8	1.5	1.5	12	7	5.3	50	50

With nine rectangle metal plates in a 3×3 layout. Planned for the 5-GHz Wi-Fi bands (4.9GHz-5.9 GHz), the antenna measurements are calculated using the full-wave simulator HFSS. The final achieved antenna measurements are illustrated in **Table 1**.

Methodology

Characteristic mode analysis of the antenna design: Characteristic mode analysis is adopted to interpret the mechanism of action of the metasurface antenna. The coaxial probe supplier is withdrawn and all other geometric measurements of the patch and metasurface are maintained identical. The characteristic mode analysis procedure can be achieved utilizing the method of moments-based characteristic mode request in commercial simulation software FEKO, where the ground plane and dielectric layers are unlimited extension in x-and y-dimensions utilizing planar multilayer substrate make. Method of moments for infinite planar multilayer substrate can be resolved using Green's functions in FEKO. For this distinctive mode structure, currents, remote fields, adjacent fields and characteristic modes requests are permitted. The measured Modal Significance (MS) of the 1st ten modes of the composition without the supplier is illustrated in **Figure 2**.

e-ISSN: 2319-9873
p-ISSN: 2347-2324

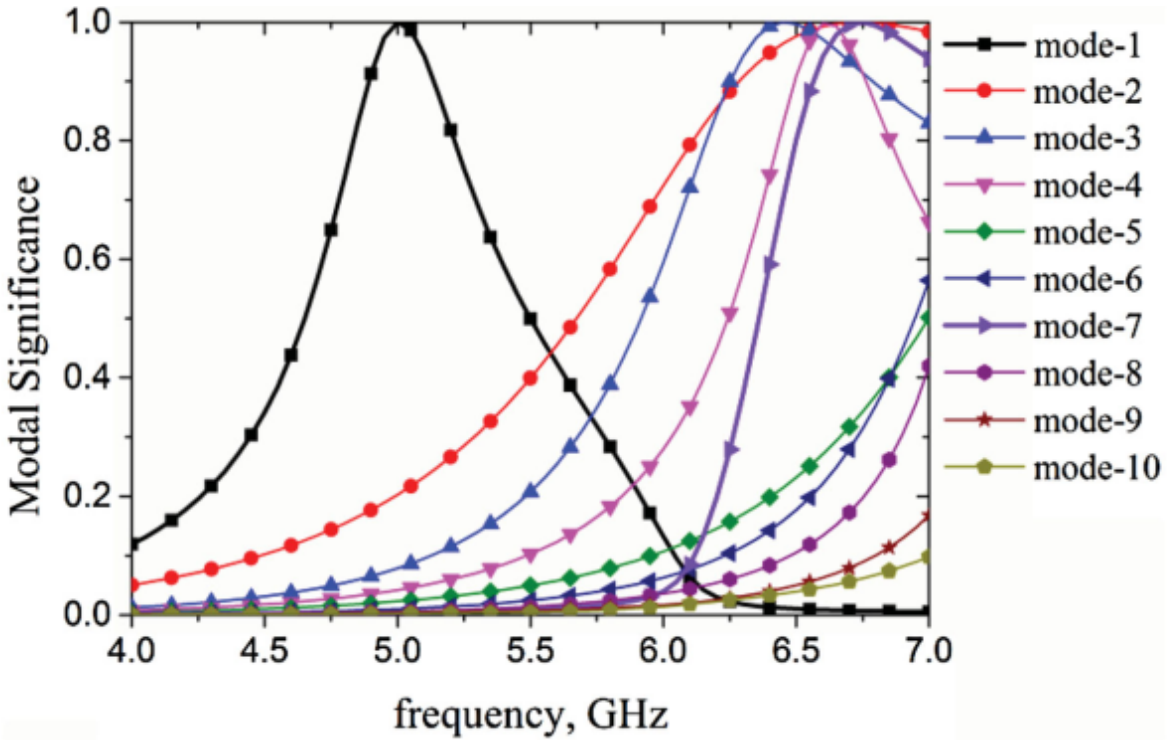

Figure 2. Modal significances of the antenna construction.

Modal current and radiation arrangement of J1-J7 is illustrated in **Figures 3 (a-g) and 4 (a-g)**.

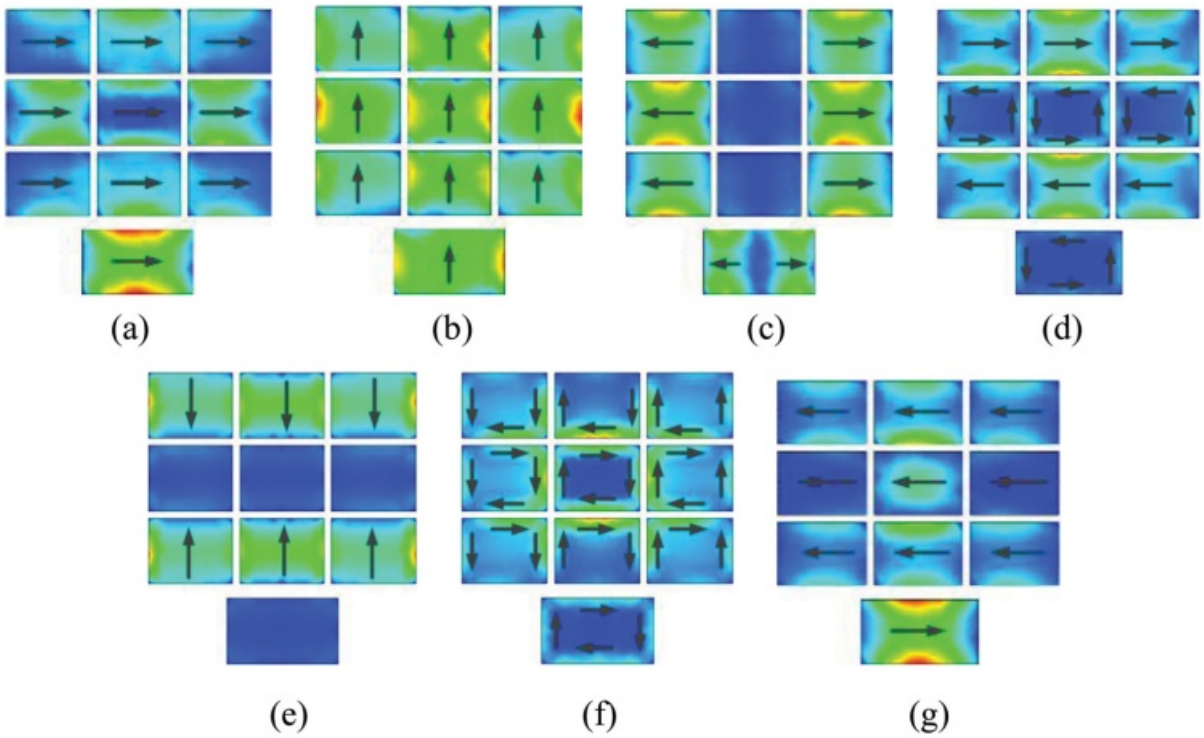

Figure 3. Modal current assessment. (a): J1 at 5 GHz; (b): J2 at 6.5 GHz; (c): J3 at 6.5GHz; (d): J4 at 6.5 GHz; (e): J5 at 6.5 GHz; (f) J6 at 6.5 GHz; (g): J7 at 6.5 GHz.

e-ISSN: 2319-9873
p-ISSN: 2347-2324

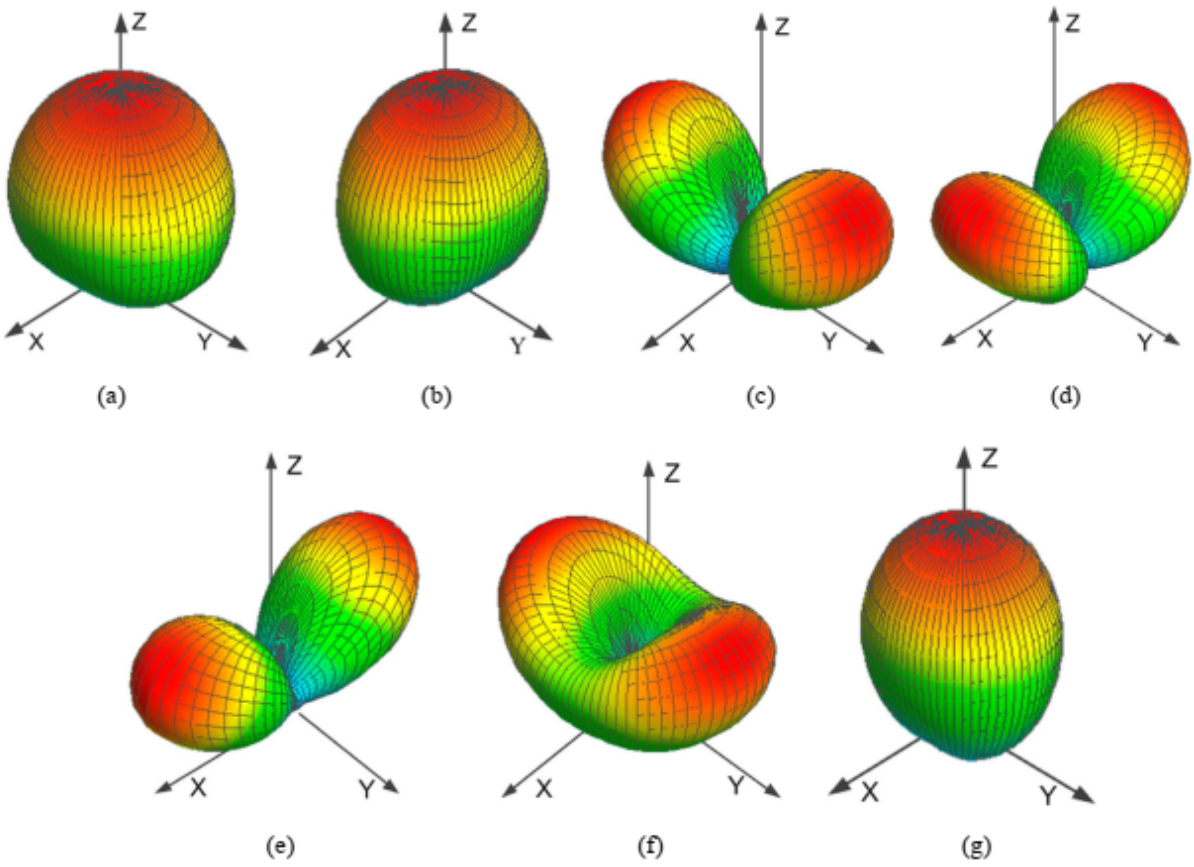

Figure 4. Modal radiation arrangement. (a): J1 at 5 GHz; (b): J2 at 6.5 GHz; (c): J3 at 6.5 GHz (d): J4 at 6.5 GHz; (e): J5 at 6.5 GHz; (f): J6 at 6.5GHz; (g): J7 at 6.5GHz.

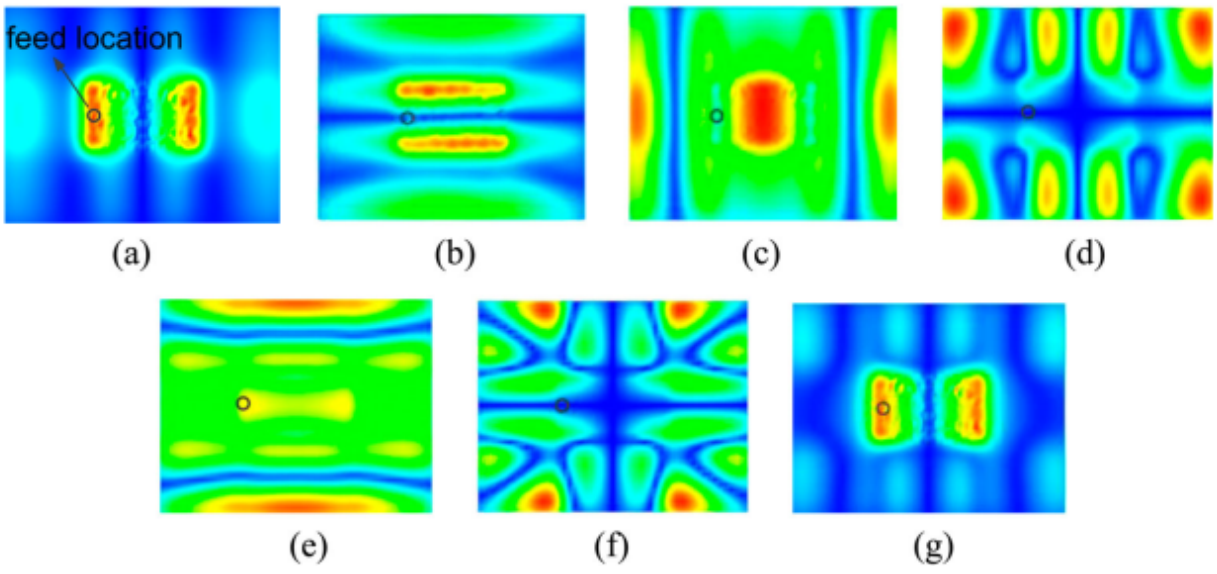

Figure 5. Modal electric adjacent-field arrangement. (a): J1 at 5GHz; (b): J2 at 6.5 GHz; (c): J3 at 6.5 GHz; (d): J4 at 6.5 GHz; (e): J5 at 6.5 GHz; (f): J6 at 6.5 GHz; (g): J7 at 6.5 GHz.

The feed point is signalled by a black circle. It can be noticed that the modal E-field of J1, J7 at the feed site is approximately maximal where the field of unwanted modes is too small **Figure 5 (a-g)**. For the coaxial probe feed by electric field coupling can be noticed as a Capacitive Coupling Element (CCE), and a random mode is stimulated capacitive if a capacitive coupling element is situated at the site of its electric field peak [34,35], J1 and J7 will be maximally stimulated **Figure 6 (a-c)**. For calculating the addition of every mode current to the whole radiated power, Modal Weighting Coefficient (MWC) with consideration to electric field coupling is measured using equation (6)

e-ISSN: 2319-9873
p-ISSN: 2347-2324

$$\left(J_{n'}E^{i}\right) = \left(E_{n'}J^{i}\right) = \int\int\int E_n \cdot J^i dv \qquad (3)$$

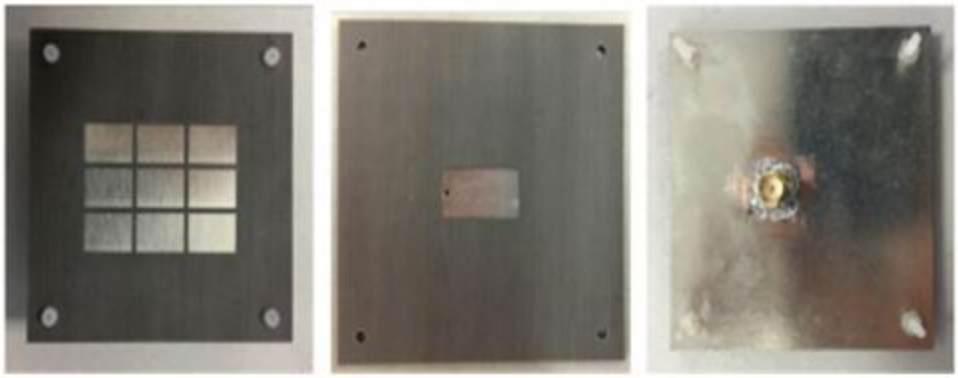

Figure 6. Photograph of the manufactured antenna. (a): Superior view; (b): Middle patch view; (c) Back view.

It can be noticed from the gained results as illustrated in **Figure 7** that J1 (at the inferior band) and J7 (at the superior band) are well stimulated, which will assist in a broadband procedure and a linear broadside radiation arrangement. Furthermore, some unwanted modes have been inhibited because of the feed situation, which will decrease the cross-polarization levels.

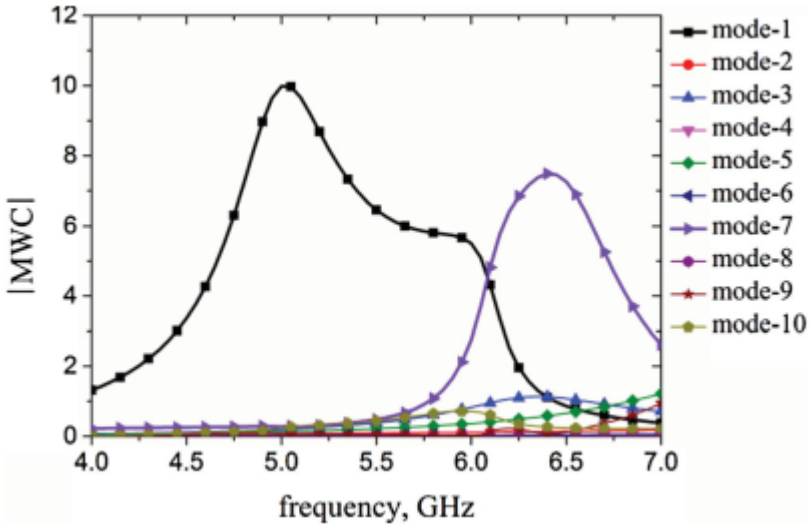

Figure 7. Modal weighting coefficient of the antenna construction.

RESULTS

The manufactured antenna is illustrated in **Figure 6**. The radiation arrangement have been simulated in full-wave simulator ANSYS HFSS 18.0 and additionally calculated in an anechoic chamber at variable frequencies. The simulated and calculated results are illustrated in **Figure 8** with good acceptance.

e-ISSN: 2319-9873
p-ISSN: 2347-2324

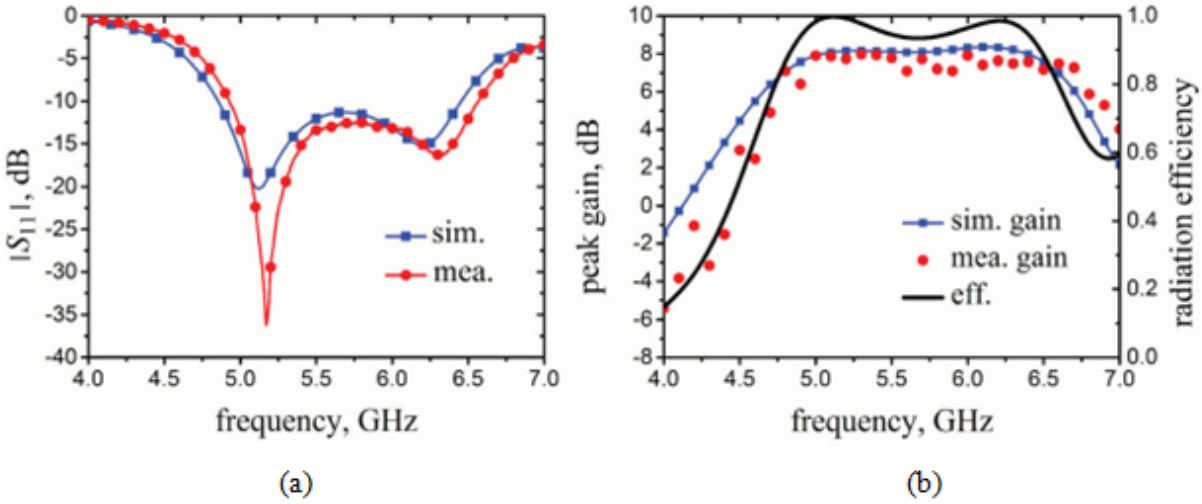

Figure 8. Simulated and calculated results. (a): Return loss; (b): Income and efficacy.

Additionally, it can be noticed from **Figures 7 and 8(a) and 8(b)** that the dual-mode wideband procedure of return loss coincides to the efficient stimulation of the 2 main modes. The calculated -10 dB impedance bandwidth is around 30% (4.89-6.62 GHz), through which the calculated peak income achieves from 6.96 to 8.21 dBi and the simulated radiation efficacy is more than 90%. Normalized radiation arrangements are shown in **Figure 9(a) and 9(b)** for 5 GHz, **Figure 9(c) and 9(d)** for 6.5 GHz.

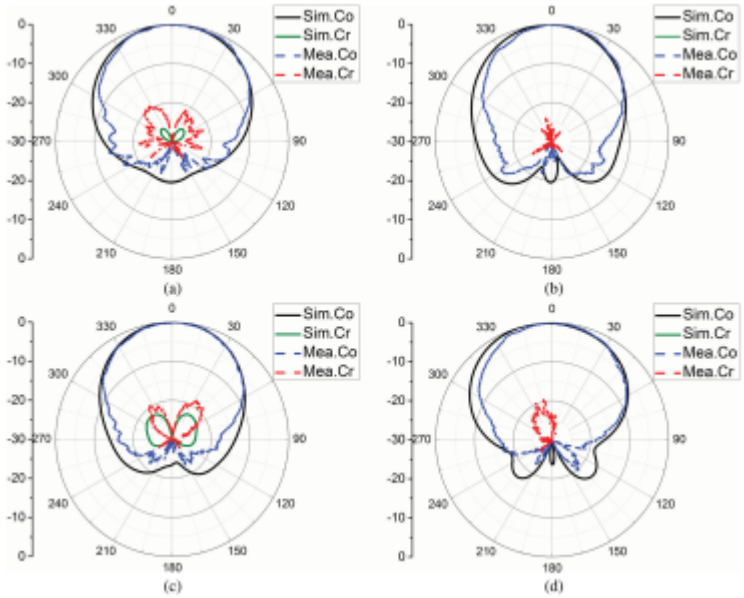

Figure 9. Radiation arrangements. (a): 5 GHz for x-z plane; (b): 5 GHz for y-z plane; (c): 6.5 GHz for x-z plane; (d): 6.5 GHz for y-z plane.

Table 2. Correlation of the act of the suggested antenna and novel dual-layer wideband patch antennas utilizing metasurface.

Antenna structures	Size (λ_{03})	-10 dB |S11| BW (%)	Efficiency	Boresight gain (dBi)
Ref (5)	1.1×1.1×0.061	25	>76%	>9.0%
Ref (11)	0.88×0.88×0.069	15	>70%	>7.5%
Ref (14)	1.05×1.05×0.06	28	>92%	>6.0%
Ref (21)	0.72× 0.72×0.075	20	>90%	>7.6%
Suggested antenna	0.95× 0.95 × 0.057	30	>90%	>6.96%

e-ISSN: 2319-9873
p-ISSN: 2347-2324

Furthermore, the cross-polarization levels are lower than 18 dB across the bandwidth because of the inhibition of unwanted modes as shown in the characteristic mode analysis procedure. The correlation of the act of the suggested antenna and several other linearly polarized metasurface antennas are illustrated in **Table 2.**

CONCLUSION

A broadband low-profile linearly polarized patch antenna utilizing metasurface for 5- GHz WiFi procedure has been intro -duced examined and analytically substantiated. The adopted coaxial probe supplier is simple to manufacture and match. CMA of the antenna construction has presented a good interpretation and description of the mechanism of action involving wideband procedure and the radiation peculiarity. The characteristic mode analysis is procedure can additionally be protracted to other patch antenna utilizing the coaxial probe feed.

REFERENCES

1. Liang Z, et al. Design and characteristic mode analysis of a low-profile wideband patch antenna using metasurface. J Electromagnetic Waves and App. 2018.
2. Wong KL. Compact and broadband microstrip antennas. 2002.
3. Matin MA, et al. Probe fed stacked patch antenna for wideband applications. IEEE Trans Antennas Propag. 2007;55:2385-2388.
4. Yang F, et al. Wide-band E-shaped patch antennas for wireless communications. IEEE Trans Antennas Propag. 2001;49:1094-1100.
5. Liu W, et al. Metamaterial-based Low-profile broadband mushroom antenna. IEEE Trans Antennas Propag. 2014;62:1165-1171.
6. Hu J, et al. A wideband quad-polarization reconfigurable metasurface antenna. IEEE Access. 2018;6:6130-6137.
7. Zhu HL, Cheung SW, Chung KL, et al. Linear-to-Circular polarization conversion using metasurface. IEEE Trans Antennas Propag. 2013;1:4615-4623.
8. Ta SX and Park L. Low profile broadband circularly polarized patch antenna using metasurface. IEEE Trans Antennas Propag. 2015;63:5929-5934.
9. Zhu HL, et al. Design of polarization reconfigurable antenna using metasurface. IEEE Trans Antennas Propag. 2014;62:2891-2897.
10. Costa F, et al. An overview of equivalent circuit modeling techniques of frequency selective surfaces and metasurfaces. Appl Comput Electromagn Soc J. 2014;29:960-976.
11. Chung KL and Chaimool S. Diamagnetic metasurfaces for performance enhancement of microstrip patch antenna. Proceedings of the 5th European Conference on Antennas and Propag. 2011.
12. Pandi S, et al. Design of scalar impedance holographic metasurfaces for antenna beam formation with desired polarization. IEEE Trans Antennas Propag. 2015;63:3016-3024.
13. Pfeiffer C and Grbic A. Planar lens antennas of subwavelength thickness: collimating leaky-waves with metasurfaces. IEEE Trans Antennas Propag. 2015;63:3248-3253.
14. Liu W, et al. Metamaterial-based low-profile broadband aperture-coupled gridslotted patch antenna. IEEE Trans Antennas Propag. 2015;63:3325-3329.
15. Costa F, et al. TE surface wave resonances on high-impedance surface based antennas: analysis and modeling. IEEE Trans Antennas Propag. 2011;59:3588-3595.
16. Liang Z, et al. Design of license plate RFID Tag antenna using characteristic mode pattern synthesis. IEEE Trans Antennas Propag. 2017;5:4964-4970.
17. Cabedo FM, et al. The theory of characteristic modes revisited: a contribution to the design of antennas for modern applications. IEEE Antennas Propag Mag. 2007;49:52-68.
18. Chen Y and Wang C-F. Characteristic-mode-based improvement of circularly polarized U-slot and E-shaped patch antennas. IEEE Antennas and Wireless Propaga Letters. 2012;11:1474-1477.
19. Obeidat KA, et al. Design of frequency reconfigurable antennas using the theory of network characteristic modes. IEEE Trans Antennas Propag. 2010;58:3106-3113.

e-ISSN: 2319-9873
p-ISSN: 2347-2324

20. Kishor KK and Hum SV. Multi-port multi-band chassis-mode antenna design using characteristic modes. IEEE Antennas and Wireless Propaga Lettr. 2017;16:609-612.
21. Manteuffel D and Martens R. Compact multimode multi-element antenna for indoor UWB massive MIMO. IEEE Trans Antennas Propag. 2016;64:2689-2697.
22. Lin FH and Chen ZN. Low-Profile wideband metasurface antennas using characteristic mode analysis. IEEE Trans Antennas Propag. 2017;65:1706-1713.
23. Lin FH and Chen ZN. A method of suppressing higher-order modes for improving radiation performance of metasurface multiport antennas using characteristic mode analysis. IEEE Trans Antennas Propag. 2018;66:1894-1902.
24. Harrington RF and Mautz JR. Theory of characteristic modes for conducting bodies. IEEE Trans Antennas Propag. 1971;19: 622-628.
25. Chen Y and Wang CF. Characteristic modes: theory and applications in antenna engineering. 2015.
26. Fang DG, et al. Discrete image theory for horizontal electric dipoles in a multilayered medium. IEE Proceedings H. 1988;135:297-303.
27. Chow YL, et al. A closed-form spatial Green's function for the thick microstrip substrate. IEEE Trans Microw Theory Tech. 1991;39:588-592.
28. Wang CF, et al. A fast full-wave analysis of scattering and radiation from large finite arrays of microstrip antennas. IEEE Trans Antennas Propag. 1998;46:1467-1474.
29. Ling F, et al. An efficient algorithm for analyzing large-scale microstrip structures using adaptive integral method combined with discrete complex image method. IEEE Trans Microw Theory Tech. 2000;48:832-839.
30. Ling F, et al. Efficient electromagnetic modeling of three-dimensional multilayer microstrip antennas and circuits. IEEE Trans Microw Theory Tech. 2002;50:1628-1635.
31. Chen Y, et al. Mixed-potential integral equation based characteristic mode analysis of microstrip antennas. Int J Antennas Propag. 2016;2016:1-8
32. Famdie CT, et al. Numerical analysis of characteristic modes on the chassis of mobile phones. Proceedings of the First European Conference on Antennas and Propag. 2006.
33. Yang B, Adams JJ. Computing and visualizing the input parameters of arbitrary planar antennas via eigen functions. IEEE Trans Antennas Propag. 2016;64:2707-2718.
34. Martens R, et al. Inductive and capacitive excitation of the characteristic modes of small terminals. Proceedings of the LAPC. 2011.
35. Martens R, et al. Selective excitation of characteristic modes on small terminals. Proceedings of the 5th European Conference on Antennas and Propag. 2011.